An Efficient Optothermal Simulation Framework for Optimization of High-Luminance White Light Sources
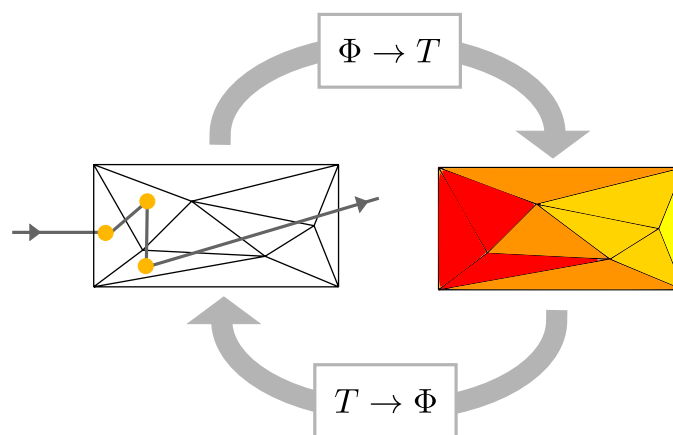
António Correia
Peter Hanselaer
Youri Meuret

An Efficient Optothermal Simulation Framework for Optimization of High-Luminance White Light Sources

António Correia, Peter Hanselaer, and Youri Meuret

Department of Electrical Engineering (ESAT) and the Light & Lighting Laboratory,
Katholieke Universiteit Leuven (KU Leuven), 9000 Gent, Belgium

Abstract: Laser diodes are very promising solid-state devices for the development of high-luminance white light sources. Currently, the most simple and efficient way to produce white light with solid-state sources is to combine them with color-converting luminescent materials or phosphors. The quantum yield (i.e., the potential to convert light to another color) of these materials has complex dependence on temperature. In the case of high-power white light sources based on laser diodes, high temperatures are reached inside the phosphor material, which decrease its quantum yield (thermal quenching) and result in a nonstable light output. While this thermal quenching effect is well known, the tools used today to design and optimize optical systems do not include it in a realistic way. This work fills that gap by proposing an automated framework that simulates both the optical and thermal effects and the interplay between them. Additionally, an adapted version of the framework is also proposed, which is more computationally efficient. The resulting shorter simulation time is crucial for the efficient optimization of the optothermal performance of lighting systems, which requires several iterations of the framework for each optimization variable. The optothermal simulation framework has been applied to some optical designs to study them by changing certain optical and thermal properties and evaluating how these affect the overall performance. It is clearly demonstrated that even for optical designs that use LED sources, neglecting the thermal effects of luminescent materials can lead to an incorrect assessment of the system's capabilities and performance.

Index Terms: Modeling, solid-state lighting applications, solid-state lighting engineered systems.

1. Introduction

The lighting industry has been increasingly adopting solid-state light sources over the last decade. This trend follows from their highly desirable characteristics such as high efficiency and longevity [1], [2]. For lighting, light-emitting diodes (LEDs) have become the most popular solid-state source. However, for applications where high-luminance is critical, such as car-headlamps, projectors, and spot/theatre lighting, laser diodes (LDs) are increasingly considered the most promising solid-state light source [3]–[5].

Both LEDs and laser diodes have a narrow emission spectrum. There are two methods available to produce white light with these solid-state sources. The first method is to combine sources with different emission wavelengths which are calibrated so that their mixing produces white light. However, because green solid-state light sources currently have poor radiant efficiency [6], this type of color mixing suffers from low efficiency. In addition, each source has different degradation dynamics and temperature dependencies, which will cause the resulting color to shift during operation. It is possible to avoid this problem by including re-calibration mechanisms to monitor and adapt the color mixing [7], but the system becomes more complex and expensive. The alternative way to produce white light is to couple an UV or blue solid-state light source with a luminescent material, a phosphor, which changes the wavelength of the incident light [8], [9]. The initial and converted colors are chosen to be complementary, so that their mixing results in white light. The amount of converted to absorbed photons, the quantum yield (QY), encodes the color conversion potential of each phosphor. The QY generally has complex dependencies on temperature, flux, and concentration.

Luminescent conversion is the method currently used to produce white light with LEDs in most general lighting applications [10]. When using this method with laser diodes, the optical flux density inside the phosphor material is much higher than what is typically obtained with LEDs [11]. Because quantum yield and wavelength conversion losses are dissipated as thermal energy, a higher optical flux inside the phosphor will inevitably lead to higher temperatures. In addition, quantum yield decreases with increasing temperature, which further increases the losses and the temperature inside the material. This effect is known as thermal quenching and it plays an important role in laser based systems because of the optical power concentration that can be obtained. The interaction between the temperature and the phosphor's quantum yield can result in complex dynamics with a profound impact on the steady-state performance. For this reason, it is pivotal to accurately include the thermal effects in the simulation tool used to design and optimize high-luminance lighting systems with laser diodes.

In the lighting community, the main tool used to study and optimize lighting systems is ray-tracing software [12], [13]. While there are several ray-tracers with specific tools for lighting, a method that realistically models thermal quenching effects is still lacking. With thermal quenching, the optical effects influence the thermal effects, which have an impact on the optical properties. Hence, it is necessary to model not only the optical and thermal properties of the system but also the interplay between these two properties. Some approaches to tackle this problem have previously been proposed. One approach proposed makes use of an analytical solution to the radiative transfer equation to calculate the optical effects coupled to a finite-element method (FEM) to solve the thermal effects [11]. This proved to be a very fast and accurate way to simulate the optical effects; however, this approach is limited to simple geometries, which restricts the range of configurations that can be tested. In other approaches, the analytical solution is replaced by a ray-tracer for the optical simulation while retaining an FEM tool for the thermal simulation [14], [15]. These approaches clearly provide greater flexibility by allowing a wider range of optical shapes to be tested when designing optical systems. However, to calculate the optical quantities inside the phosphor these approaches rely on a voxel-based discretization, which is a very poor approximation when using curved geometries. In addition, the thermal simulation solves the steady-state equation, effectively discarding the interplay effects between the thermal simulation and the optical simulation, which are at the heart of thermal quenching. A similar opto-thermal coupling has been proposed that solves the transient heat equation instead of using the steady state solution [16]. Similar to the previous approaches, the impact of the thermal effects on the quantum yield is disregarded, making it impossible to simulate thermal quenching.

To cover the gap in the approaches that have been proposed so far, an automated framework that models the optical and thermal effects and considers the interplay between them is presented. The framework relies on commercially available tools to model each individual effect, but extends them so they are able to simulate the opto-thermal interplay. Any material property that influences the opto-thermal feedback (e.g., refractive index, quantum yield) can be introduced into the framework and modelled. This work focuses on thermal quenching, which is modelled by

only considering changes in the quantum yield. This allowed optimizing the framework resulting in significant computational performance improvements that are crucial when trying to optimize a lighting system, which is a very computationally demanding task. The framework is applied to study the performance of remote phosphor configurations, i.e., lighting systems where the phosphor is not in direct contact with the light source. This type of system is more compatible with laser diodes than conformal phosphor coatings that are directly applied onto the light source. This makes remote phosphor configurations the most relevant case to analyze in this study.

2. Methods

2.1. User-Created Phosphor Particle

LightTools (Synopsys, Inc., CA, USA) is a powerful ray-tracing tool that is widely used for the simulation of optical systems. Despite its extensive features for lighting applications, it is not able to comprehensively model the thermal quenching effects in luminescent materials. For that it is necessary to be able to define optical properties spatially and to store the volumetric distribution of the absorbed optical flux. The absorbed flux distribution can then be used in a thermal simulation tool as a heat source to simulate the temperature evolution inside the phosphor and calculate an updated quantum yield distribution. This, in turn, when used in LightTools, will allow to obtain a new absorbed optical flux distribution that takes into account the increase in temperature. The ability to store and read material properties spatially can be introduced in LightTools by implementing an user-created phosphor particle. In LightTools, scattering and luminescent materials are modelled by creating a host material and assigning to it a specific particle type. Both volume scattering and luminescent effects have a corresponding particle type, which can be parametrized (e.g., define mean free path or specify the absorption spectrum). For these cases, the full ray-tracing behavior inside the material is already implemented in LightTools. However, for user-created particles, the ray-tracing inside the material is not implemented, thus it was necessary to design and implement computer routines to handle volume scattering and luminescence effects. Essentially, a ray-tracer was implemented for the inside of the phosphor to mimic the built-in particle's ray-tracing behavior and extended to define and store properties spatially.

The algorithm implemented follows the main concepts of the classical Monte-Carlo ray-tracing method [17], [18], while extending its behavior to handle luminescence. While being traced, a ray may interact with the phosphor material and be either scattered or converted. In a scattering event, only the incident ray's trajectory is changed. The deflected direction is statistically sampled from a phase function model supplied by the user. In a conversion event, the material's quantum yield defines which part of absorbed ray's flux will be attributed to a new ray with a new wavelength and which part will be lost as heat. The converted wavelength is chosen by sampling the material's emission spectrum. This wavelength conversion leads to an optical energy loss (Stokes shift loss), generating heat. The total absorbed flux Φ_a that is lost as heat at each conversion event location u is given by (1), shown below. The first term corresponds to the quantum yield losses and the second term represents the Stokes shift losses related to conversion between the incoming wavelength λ_{in} and the outgoing wavelength λ_{out}

$$\Phi_a(u) = (1 - QY(u))\Phi_{in} + \left(1 - \frac{\lambda_{in}}{\lambda_{out}}\right)QY(u)\Phi_{in}$$

$$= \left(1 - \frac{\lambda_{in}}{\lambda_{out}}QY(u)\right)\Phi_{in}. \tag{1}$$

The ray-tracing behavior of the user-created particle was validated by comparing it to the behavior of a built-in LightTools phosphor particle. The validation configuration was built in LightTools and consists of a cylindrical object to which both a built-in phosphor particle, and the user-created particle were assigned to and sequentially tested. The full domain can be seen in Fig. 1 and consists of the cylindrical phosphor (in yellow) and a blue light emitting surface source (in blue). The
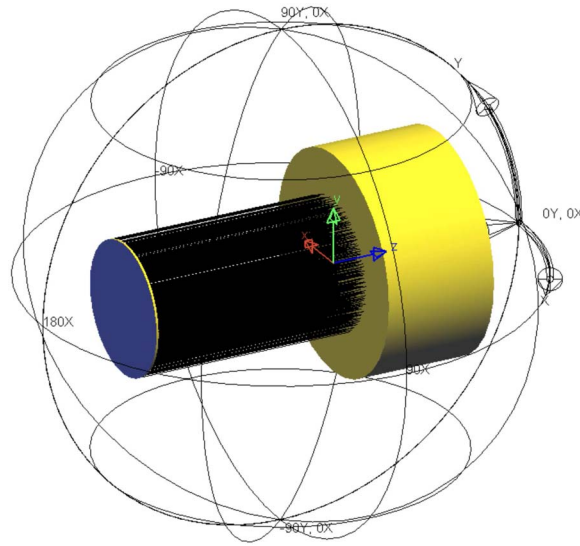
Fig. 1. Validation domain with the source (blue surface) positioned on the left emitting light toward a phosphor cylinder (in yellow). The phosphor cylinder is 0.5 cm thick and has a radius of 0.5 cm. The scattered rays were hidden so that the configuration's geometry is not obscured.
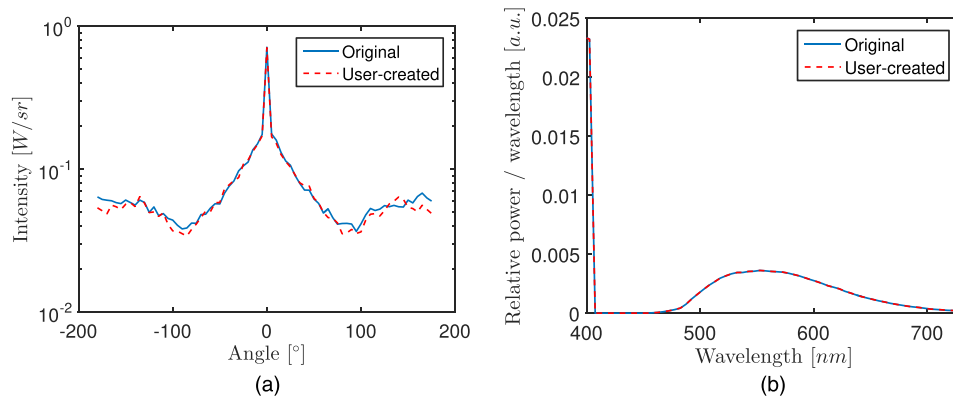

Fig. 2. Comparison between the built-in phosphor particle and the user-created particle regarding their (a) far-field intensity patterns (logarithmic scale) and their (b) wavelength resolved power distributions.

volume scattering and spectral properties of YAG:Ce, which is the most popular phosphor used in lighting applications, were obtained from the literature [19], [20] and supplied to both particles. The quantum yield was fixed at QY = 0.92 for all wavelengths. The mean free path and albedo were calculated using a scattering coefficient of $\mu_s = 8.0$ mm^{-1} and an absorption coefficient of $\mu_a = 3.0$ mm^{-1}. The angular deflection was modelled using a Henyey–Greenstein phase function with asymmetry parameter $g = 0.8$. The pseudo-random number generator seed was kept fixed between simulations so that the validation could be done with minimal random sampling noise. For each 1×10^6 ray simulation, the far-field intensity distribution and the wavelength-resolved power distribution were stored for comparison.

The far-field intensity patterns for the built-in and the user-created particles are very similar, as shown in Fig. 2(a). In Fig. 2(b), the power spectrum of both particles is shown to overlap. These results demonstrate that the basic ray-tracing algorithm implemented produces essentially the same results as LightTools' own implementation.
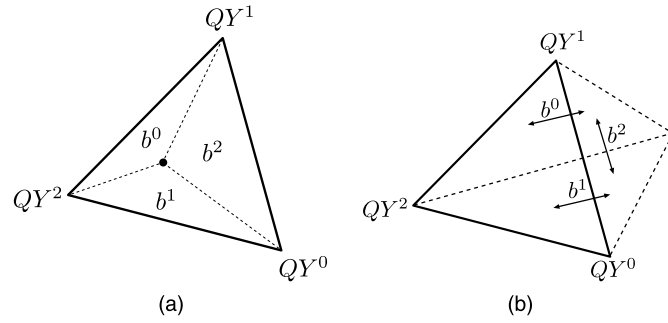
Fig. 3. Example of barycentric coordinates for a (a) point inside a triangle and a (b) point outside a triangle. In (b), the barycentric coordinate b^2 is negative, whereas b^1 and b^0 are positive.

To include thermal quenching effects, the user-created phosphor particle was extended to store the absorbed optical flux (the optical power lost as heat) and to define the material properties spatially: specifically the QY. To accomplish this, a tetrahedral element discretization of the phosphor material that stores material properties at the elements' nodes (vertices) was adopted. Using a tetrahedral element mesh increases the modelling accuracy when using complex geometries and widens the range of thermal simulation tools that can be efficiently coupled to the optical simulation. To include the mesh, some changes to the user-created particle were necessary. Since the QY is stored at the mesh's nodes, it is necessary to identify inside which element a conversion event takes place. Additionally, the value of the QY at the event's location (inside the element) needs to be computed from the QY values at the nodes. To solve both problems simultaneously, barycentric coordinates were used [21]. To calculate the barycentric coordinates, the event's location is used as a test point and conceptually divides a tetrahedral element into four new elements, each using the test point as a vertex. The barycentric coordinates between the test point and the test element are simply the volume of each of the new elements normalized by the original element's volume. If the barycentric coordinates b^i between a point and an element are bounded as $0 \leq b^i \leq 1$, then the point is inside that element. To better clarify this property, a simpler 2-D case that uses triangles instead of tetrahedra is illustrated in Fig. 3. This property is tested when calculating the barycentric coordinates between a conversion event's location and each tetrahedral element in the mesh to find the containing element. Additionally, using the barycentric coordinates, the value of the QY at any point inside the element can be linearly interpolated from the QY values at the nodes QY^i using (2). With this interpolation method, the material properties are automatically defined in a continuous way inside the material. This property is very advantageous and it is the reason why a node based approach was preferred instead of considering the mesh values at the tetrahedral elements' centre. After each conversion event, the absorbed flux can be stored at the nodes using the barycentric coordinates as weights. To calculate the contribution of an event's absorbed flux to each node of the containing element, (3), shown below, is used

$$QY(u) = b^0 QY^0 + b^1 QY^1 + b^2 QY^2 + b^3 QY^3 \tag{2}$$

$$\Phi_a^0 = b^0 \Phi_a(u) \quad \Phi_a^1 = b^1 \Phi_a(u)$$
$$\Phi_a^2 = b^2 \Phi_a(u) \quad \Phi_a^3 = b^3 \Phi_a(u). \tag{3}$$

The inclusion of the tetrahedral mesh into the ray-tracing software significantly reduces its performance. Determining which tetrahedral element encloses the event's location using the barycentric coordinates is the main performance bottleneck. This was mitigated by restricting the set of elements to test using barycentric coordinates. Each element's minimum bounding box is supplied to the ray-tracing software and used to quickly bypass all elements whose volume

does not include the event's location. As this test is faster than calculating and testing the barycentric coordinates, the overall simulation speed increases.

2.2. Opto-Thermal Framework

Running an optical simulation in LightTools with the user-created phosphor particle returns the distribution of the absorbed optical flux $\Phi_a(u)$ (in W) inside the phosphor material. This needs to be normalized by the volume to obtain a thermal power density distribution $Q(u)$ (in W/m^3), which can be used in a thermal simulation tool as a heat source. To perform the normalization, the absorbed flux at each node n is divided by its barycentric volume V^b. This is calculated by accumulating the volume contributions from all N elements that share node n, resulting in

$$Q^n = \Phi_a^n(V^b)^{-1} = \Phi_a^n\left(\sum_{k=1}^{N}\frac{V_k}{4}\right)^{-1}. \tag{4}$$

The thermal simulation is performed with COMSOL (COMSOL, Inc., MA, USA). The calculated thermal power density distribution is stored in the original tetrahedral mesh, which can be directly used with COMSOL. Sharing the same mesh between optical and thermal simulations avoids approximation or binning errors. To perform a simulation in COMSOL, the geometric and material properties of the optical system need to be modelled inside COMSOL. Only the elements which have an impact in the thermal properties of the system are modelled in COMSOL. For instance, an aluminium reflector in contact with the phosphor may act as a heatsink, therefore it would be a relevant element in the thermal simulation. However, a lens system that is not in contact with the phosphor is unlikely to have an impact on its thermal properties, therefore it is not considered in the thermal simulation. Every material that is in direct physical contact is assigned thermal contact boundary conditions in the thermal model. Any surface that faces a relatively large open domain, has convection boundary conditions assigned to it which are modelled using the heat transfer coefficient h. This coefficient depends only on the cooling medium's properties (e.g., velocity of the surrounding air) and not on the material's properties. The remaining surfaces may only dissipate heat through radiation and, therefore, are assigned radiative boundary conditions. The room temperature, which is used to calculate the dissipative contributions at the boundaries, is fixed at 293 K.

A simplified flowchart of the framework is shown in Fig. 4(a). After having defined the model for the full optical system in LightTools and the model for the representative thermal system in COMSOL the framework can be used. Each iteration starts with an optical simulation in LightTools to obtain the thermal power density distribution mesh Q. This mesh is then used in COMSOL as a volumetric heat source, which solves the transient heat equation [(5)], subjected to the boundary conditions described previously. The mass concentration ρ, volume heat capacity C_p, and thermal conductivity k are modelled as scalar quantities for each material

$$\rho C_p \partial_t T = k\nabla^2 T + Q. \tag{5}$$

Every iteration of the thermal simulation results in an updated temperature distribution. From it, a corresponding quantum yield distribution is calculated using (6), shown below. The phosphor material's radiative lifetime τ_r is assumed to not change significantly with temperature when compared to the nonradiative lifetime τ_{nr}. To calculate the temperature dependent nonradiative lifetime $\tau_{nr}(T)$ for YAG:Ce, (7), shown below, was used in all simulations performed. This equation stems from an empirical formulation obtained by fitting experimentally obtained data to the Arrhenius equation [11]. In this equation, k_B is the Boltzmann constant and the fitted W_0 (4×10^{13} s^{-1}) and E_0 (6.5×10^3 cm^{-1}) parameters were obtained from the literature [22]. If the updated quantum yield does not significantly change between consecutive steps (e.g., $\Delta QY < 0.01$), the thermal simulation is extended. If the QY significantly decreases, the updated QY distribution is passed on to LightTools to perform a new optical simulation. This

Fig. 4. Flowchart of the framework for the (a) general case and for the (b) vectorized approximation showing example values for the stopping conditions. Full LightTools refers to simulating the entire domain with LightTools, whereas quick LightTools refers to using the artificial source to bypass the phosphor simulation.

condition is used because a small difference in the QY distribution will not significantly change the result obtained with the optical simulation. If the optical simulation outputs (e.g., color coordinates, luminance distribution) are required at shorter time intervals, this condition can be relaxed at the cost of longer simulation times:

$$QY(T) = \tau_{nr}(T)(\tau_{nr}(T) + \tau_r)^{-1} \qquad (6)$$

$$\frac{1}{\tau_{nr}(T)} = W_0 \exp \frac{E_0}{k_B \, T}. \qquad (7)$$

The framework's iterative cycle is repeated until any one of the two following conditions is met. The ideal condition is if the system is close to reaching a steady state, which is implemented by comparing the value of the time derivative of the temperature to a user-defined threshold (e.g., $\partial tT < 0.1$ K/s). The other condition is when the mean quantum yield is too low, which implies that the system is no longer producing white light (e.g., $\overline{QY} < 0.5$). Different threshold values for the stopping criteria can be used, in order to have stricter stopping conditions, improving the simulation accuracy but decreasing the simulation speed.

The proposed general framework couples the optical and thermal dynamics of any optical system and it is able to simulate the influence of the optical effects on the thermal effects and vice-versa. This allows to investigate the influence of the material properties on the system's overall performance. If the dependence on temperature of other material properties is available (e.g., refractive index), they can be easily included and modelled. Because of its coupled nature, the framework can supply any metric that is calculated with either COMSOL or LightTools along with their temporal dynamics.
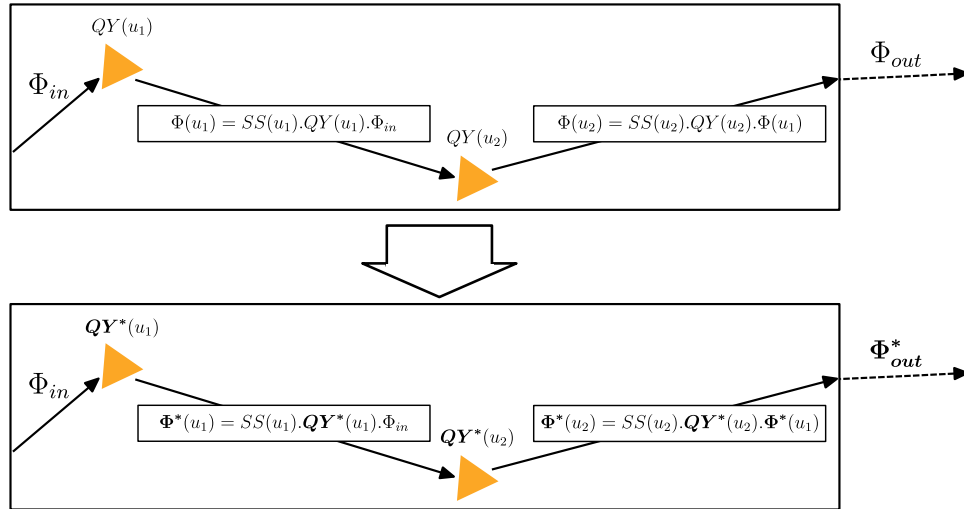
Fig. 5. Upper illustration shows the initial ray tracing, whereas the bottom illustration shows the effect of updating the QY. Using these QY values (superscript *), the losses and updated exiting flux Φ_{out}^* can be computed. The temperature impacts the QY values, but does not alter the ray direction and Stokes shift (SS) losses at each conversion event.

2.3. Vectorized Opto-Thermal Framework

The framework proposed above can be simplified if thermal quenching is the main effect to be modelled. In the optical simulation, the change in QY impacts the magnitude of the absorbed flux distribution. In essence, the flux of each traced ray will be different due to the change in QY, however, each ray's trajectory and converted wavelength will not change. This simple fact allows simplifying the general framework into a new framework shown in Fig. 4(b), which is computationally more efficient. As the quantum yield's dependence on temperature is the main effect in thermal quenching, this framework still realistically simulates thermal quenching effects.

In the simplified framework, the optical simulation is run only once and the ray information at conversion events is stored along with the volumetric distribution of absorbed flux. The rays at the exiting surface of the phosphor material that will not re-enter it are also stored. Then, as before, a thermal simulation is performed. However, the resulting updated quantum yield is no longer used with LightTools. Instead, it is used, along with the ray information at conversion events, to compute the updated flux distribution directly. This is calculated by updating only the QY losses at each conversion event, changing the outgoing flux and propagating it to subsequent conversion events. A depiction of this process is shown in Fig. 5. All other ray data remains the same, including the Stokes shift losses $(SS(u))$ and the ray deflection angles. Since for each ray the sequence of conversion events is fully independent of other rays, the calculations can be grouped together. Because these involve applying the same operations to blocks of data, the computation can be performed by taking advantage of vectorized instructions, greatly decreasing the computation time. The updated absorbed flux distribution is then normalized to obtain the thermal power density distribution which is used in COMSOL. By updating the losses, the optical flux of light exiting the phosphor can also be directly updated. This is used to create an artificial source at the exiting surface that only emits rays that reach the detector and can't influence the phosphor again. Essentially, this bypasses the need to perform any further complete LightTools simulations, i.e., a simulation that includes the full ray-tracing inside the phosphor. Instead, a quick LightTools simulation can be performed which only traces rays from the artificial source to the detector to obtain all the outputs that can be usually obtained with LightTools (e.g., far-field intensity distributions, color quality metrics). Calculating the updated absorbed flux with the vectorized mode is much faster than running a ray-tracing simulation. For a 1×10^6 ray simulation of a phosphor, a full LightTools simulation takes about 76 seconds,
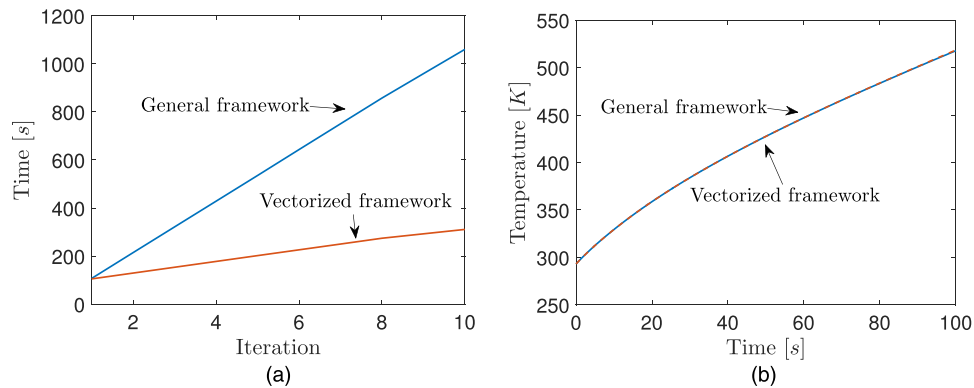
Fig. 6. Comparison between the general and vectorized framework regarding (a) total simulation time and (b) simulated temperature dynamics.

TABLE 1

Values of the thermal properties used in the simulations

Domain	Thermal conductivity W/(m.K)	Heat capacity J/(kg.K)	Density kg/m^3	Emissivity
Reflectors	238	900	2700	0.90
Silicone phosphor	0.4	1150	1800	0.92
Glass phosphor	1.4	703	2203	0.90

while a quick LightTools simulation takes up to 0.8 seconds. The more rays are traced, the bigger this gap becomes, since LightTools' performance is very dependent on the number of rays traced. As each iteration of the framework includes a LightTools simulation, this speed-up becomes more significant as more framework iterations are needed. For the validation configuration used (shown in Fig. 1), the cumulative simulation time is plotted in Fig. 6(a). For 10 iterations of the opto-thermal framework, the total simulation time decreased from around 18 minutes with the general framework to approximately 3 minutes with the vectorized framework. The increase in efficiency achieved becomes more significant when considering that to optimize optical configurations, several iterations need to be performed for each optimization variable. This way, the vectorized framework can be used to automatically and efficiently optimize opto-thermal configurations by navigating through a list of possible changes and simulating their impact on the overall system performance.

The vectorized framework was validated against the general framework using the validation configuration described before. As it consists of a cylinder facing an open domain, convective and radiative boundary conditions were applied to all of its surfaces and a convective heat transfer coefficient of $h = 5$ W/(m.K) was used. The phosphor plate consists of a blend of silicone and YAG:Ce phosphor, whose thermal properties are described in Table 1. In Fig. 6(b), the evolution of the maximum temperature obtained with each framework is shown to overlap. Because this evolution depends on both the optical and thermal simulations and their interplay, this clearly shows that the vectorized approach returns the same results as the general approach.

3. Results

A comprehensive test of the framework developed was performed to demonstrate its capabilities and its flexibility when applied to analyze and optimize the thermal and optical properties of configurations of high-luminance white light sources. For this test, an extension of the validation configuration was modelled, as depicted in Fig. 7. The phosphor plate is 0.2 cm thick and has a radius of 1 cm. Five light sources are distributed inside a reflecting aluminium mixing cavity
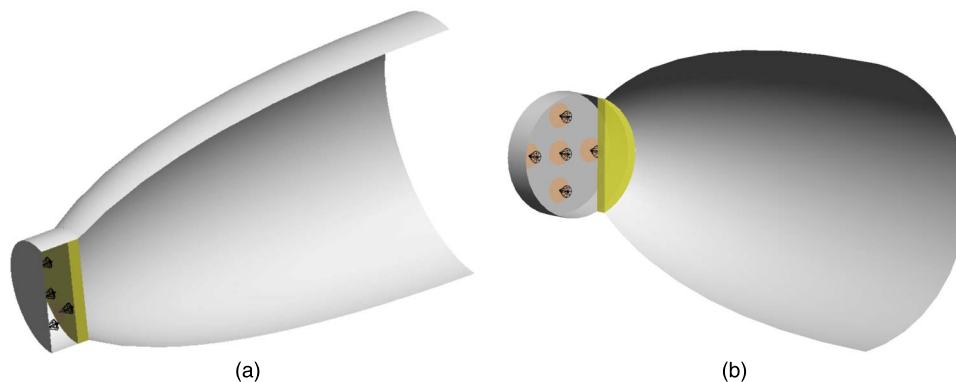
Fig. 7. Simulation domain (a) cropped longitudinally and (b) rotated to show the light sources' location inside the mixing cavity.

0.5 cm long, with a radius of 1 cm. In addition, an aluminium compound parabolic concentrator (CPC) is used as a collection optic to restrict the angular extent of the light produced by the system to 25°. The phosphor material's thermal properties were established assuming a blend of silicone and YAG:Ce in one scenario and a YAG:Ce silica glass in another. The values for the thermal properties of the materials that are used in the system are described in Table 1. The values for the phosphor mixtures were based on the thermal characteristics of the substrate, as the added phosphor particles have a marginal impact on those characteristics.

The opto-thermal simulation framework was used to investigate the effect of various changes in the optical system. These include modulating the output power of the light sources, using either LEDs or laser diodes as sources, using different phosphor materials and changing the cooling solution (e.g., adding a fan). The output optical power of each source was varied as $P = \{1, 3, 5\}$ W. The heat transfer coefficient for all convective boundaries was changed from $h = 5$ W/(m.K) for passive cooling to $h = 25$ W/(m.K) for active cooling. A LED was modelled as a source with Lambertian radiant intensity with an angular extent of 85° and a laser diode as a light source with uniform radiant intensity with a 5° angular extent. Both sources' emission spectra have a central wavelength of 457 nm and a bandwidth of 3 nm. While the bandwidth is atypically narrow for a LED, it will not impact the investigation of the framework's performance and capabilities. The thresholds for the framework's stopping criteria were significantly relaxed for this test so that the long-term behavior of the simulations could be obtained. This enables obtaining output metrics even when the light sources are no longer able to produce white light. To still have practical simulation times, an additional stopping criterion was implemented that stops the framework if the maximum temperature inside the phosphor reaches 1000 K.

3.1. Silicone-Phosphor Material

First, the maximum temperature reached in the silicone-phosphor blend material was investigated when using either five LED sources or five laser diodes. As shown in Fig. 8, the LD configuration clearly reaches much higher temperatures than the LED configuration in a shorter amount of time. The thermal and optical interplay that is caused by thermal quenching can be clearly seen in Fig. 8 (for the 3 W and 5 W cases) when the temperature reaches around 600 K. At this point, due to the increase in temperature, the quantum yield decreases strongly, which leads to a sharp increase in temperature (thermal runaway). For the 5 W case in Fig. 8(a), the temperature slope begins to decrease later in the simulation due to convective and radiative dissipation. These mechanisms would also influence the temperature slopes of the 3 W and 5 W cases in Fig. 8(b) to decrease, but at much higher temperatures. However, at this stage the temperature would already exceed the damage threshold of the phosphor mixture. In the same figure, it is also shown that the cooling regime (passive or active) has virtually no effect on the
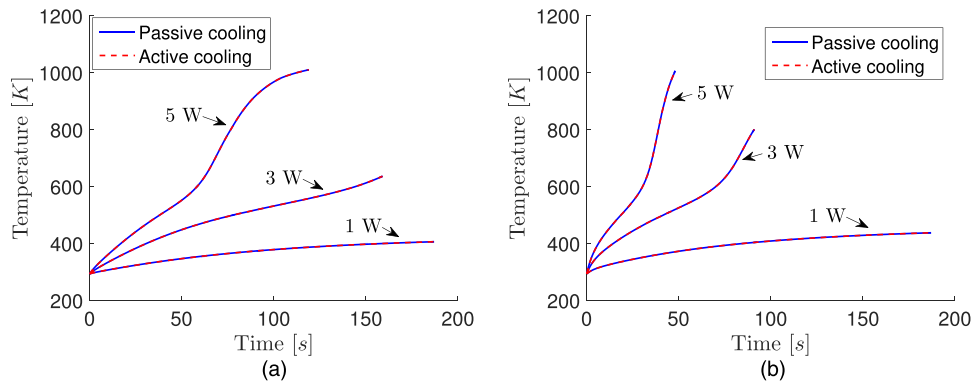
Fig. 8. Maximum absolute temperature dynamics inside the silicone-phosphor material for all optical output powers tested under different cooling conditions of (a) five LEDs and (b) five LDs.
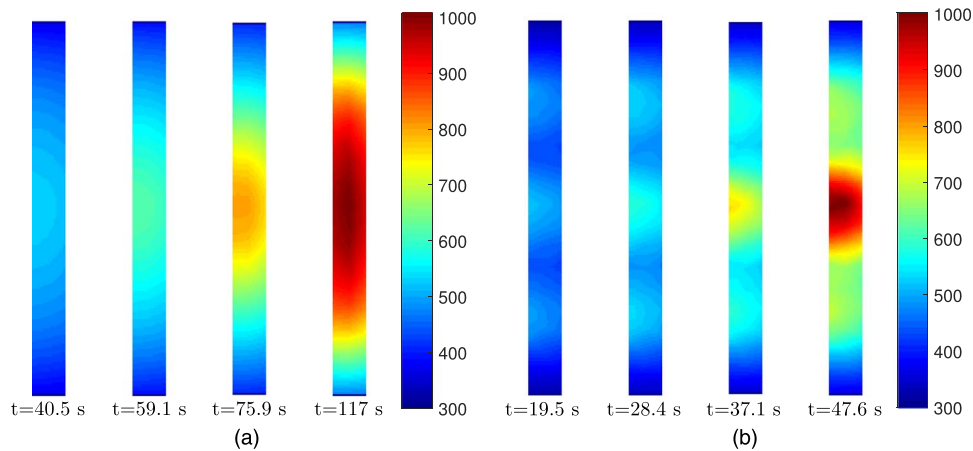

Fig. 9. Absolute temperature distribution in a cross section of the silicone-phosphor material over time under passive cooling for (a) five 5-W LEDs and (b) five 5-W LDs. Cross-section dimensions are 2 cm × 0.2 cm.

temperature dynamics. This is caused by the silicone-phosphor blend's poor thermal characteristics and the small area of contact between the phosphor and the aluminium cavity. In Fig. 9, the spatial distribution of the temperature inside the phosphor is depicted at different times during the simulation. While the contribution of three of the five different sources can be seen in the first steps of the simulation, the temperature becomes concentrated in the middle, away from the convective boundaries of the aluminium mixing cavity. As expected, the simulation of the laser diode scenario results in the sharpest temperature gradients.

The luminous efficacy, which in this work is defined as the ratio of the output luminous flux of the system to the optical output power of the solid-state light sources, is plotted for each case in Fig. 10. Both LED and LD cases show a significant decrease in luminous efficacy for the 3 W and the 5 W sources. Similarly to the temperature dynamics shown before, the efficacy drops faster and more sharply in the LD systems than in the LED systems but remains stable in both when using the 1 W sources. Luminance maps are collected at the CPC's exit and used to calculate the average luminance over time, which is shown in Fig. 11. As expected, increasing the output power of the sources increases the system's luminance up until a certain point when thermal quenching effects become significant and quickly lower the efficiency. Finally, true color maps of the far-field intensity are shown in Fig. 12 to demonstrate the angular distribution of the color of the light produced by the system. In the upper row, the angular distribution of the light
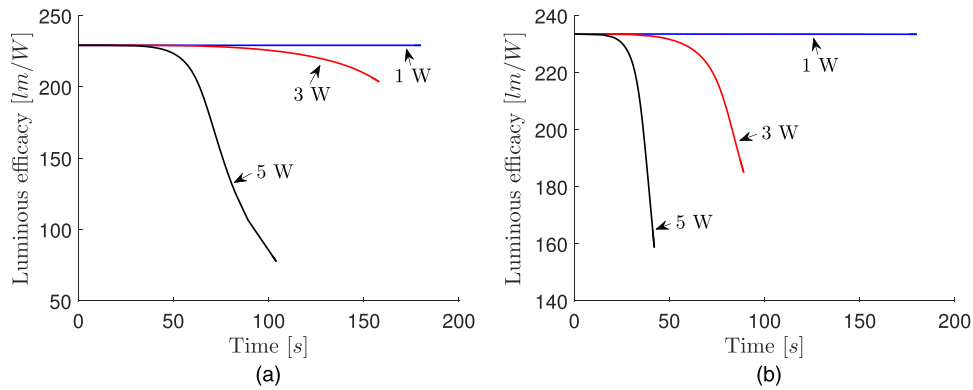
Fig. 10. Total luminous efficacy obtained for different optical output powers of (a) five LEDs and (b) five LDs.
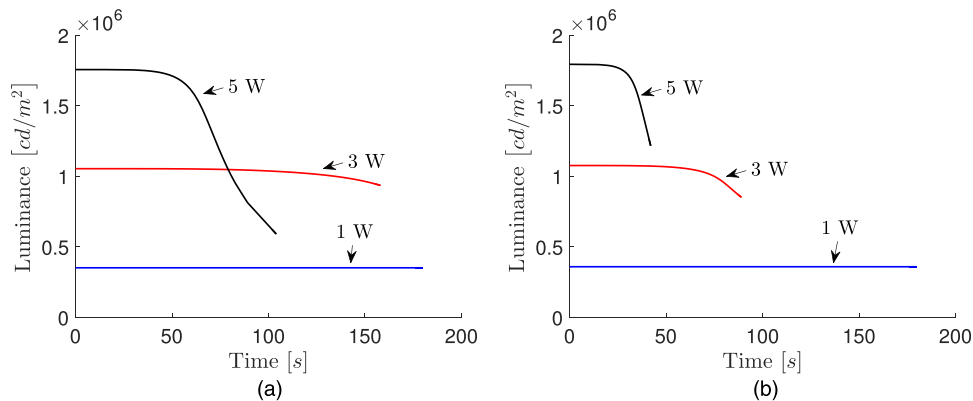

Fig. 11. Average luminance obtained under passive cooling for different optical output powers of (a) five LEDs and (b) five LDs.

emitted using only LEDs shows a smooth color distribution in the beginning, but progressively becomes more blue. This is a clear consequence of the sharp decrease of the mean quantum yield in the phosphor due to the increase in temperature. Interestingly, the laser diode scenario plotted in the bottom row shows only a marginal deterioration of the white light produced throughout the simulation. This is because the simulation of the laser diode scenario stopped because the system reached a maximum temperature of 1000 K. Because of the sharp temperature gradient, the mean temperature was significantly lower, unlike the LED case, where the maximum and mean temperatures are similar. This way, the off-centre sources were still incident on a part of the phosphor material which was relatively cool and still retained a high QY. Because of the mixing in the collimation optics, the converted light of the off-centre sources compensated the shortcomings of the on-center source that was emitting blue light that travelled through the phosphor without being converted.

Even for this simple optical system, these results show the importance of considering thermal quenching. As shown, even the cases which use LEDs as light sources may be limited by thermal effects and their influence on the phosphor material. A thermal analysis that disregards these effects will always underestimate the temperature reached inside the phosphor. The wrong assessment of the system's dynamics renders the optimization stage useless, as the outputs driving the optimization are inaccurately calculated. Any optical design that is optimized that way may result in a system that produces non-stable white light.
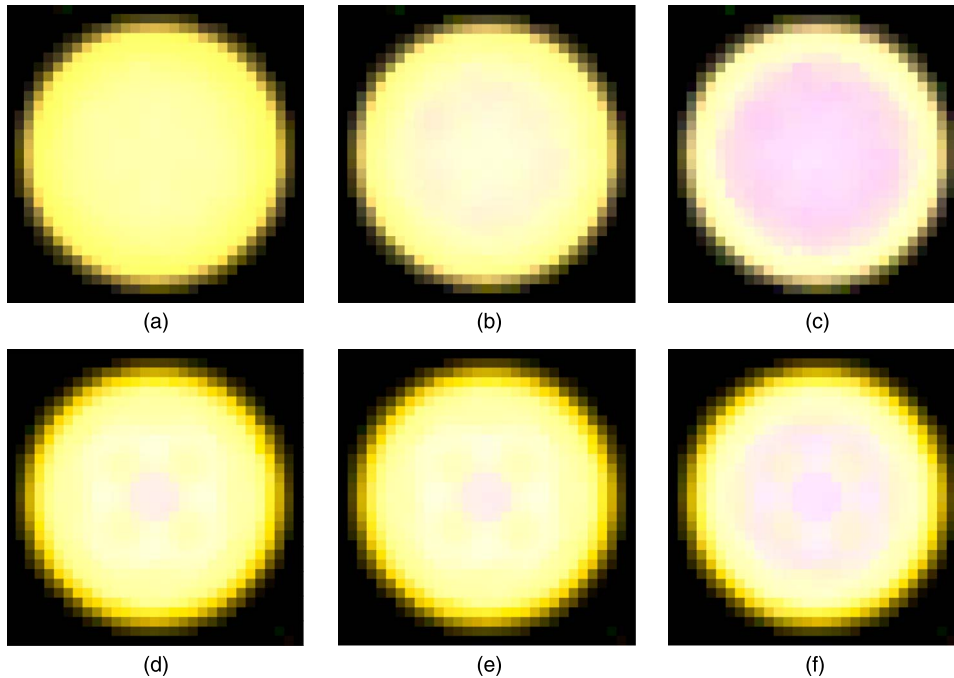
Fig. 12. True color images of the far-field intensity for the (a)–(c) five 5-W LEDs at three different periods of the simulation. (d)–(f) show the same for five 5-W LDs.
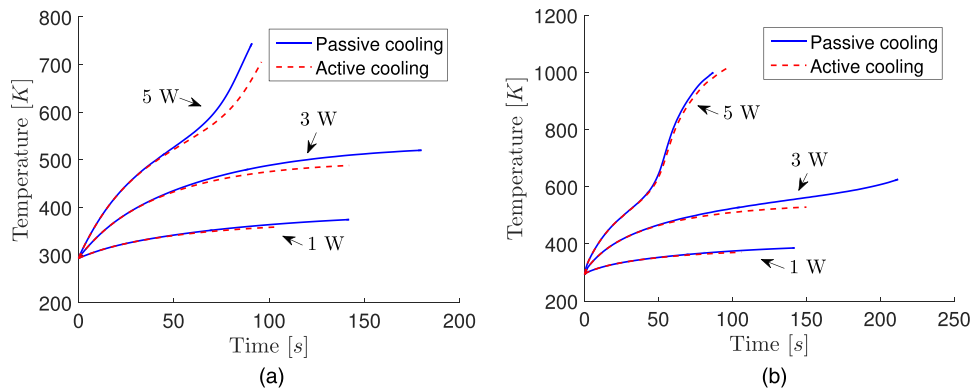

Fig. 13. Maximum absolute temperature dynamics inside the glass-phosphor material under passive and active cooling for different optical output powers of (a) five LEDs and (b) five LDs.

3.2. Glass-Phosphor Material

For the simple system analyzed in the previous section, the thermal properties of the silicone-phosphor material were the main factor limiting the system's performance. Without changing the geometry, the silicone based material was replaced by a glass-phosphor material, which has overall better thermal properties, and the system performance was re-analyzed. The temperature evolution for all cases is presented in Fig. 13. Clearly, the glass-phosphor material improves the thermal performance of the system. When changing the cooling solution, there was a more pronounced dissipative effect, which becomes significant for some of the configurations tested. In Fig. 13(b), the 3 W laser diode case shows an entry point into a thermal quenching regime which is avoided when applying an active cooling strategy. The increased impact of the cooling strategy used is a direct consequence of the better thermal properties of the glass-phosphor material.

These comprehensive tests done with the opto-thermal simulation framework show that it solves the thermal and optical effects in an efficient way and demonstrate that it can be used to have a more realistic prediction of a system's performance.

4. Conclusion

An efficient framework which simultaneously simulates the optical and thermal properties of luminescent materials in optical systems is presented. This framework accounts for the interplay between optical and thermal effects which is crucial to simulate thermal quenching effects of phosphors in a realistic way. This is a powerful tool to automatically investigate the influence of dissipation mechanisms, material properties and component geometry on the system's real performance. To exclusively study thermal quenching, an optimized version of the framework is also presented and shown to computationally more efficient. The increased performance allows using the framework to efficiently optimize the opto-thermal characteristics of optical systems, which is increasingly important in high-luminance white light source design.

The capabilities and versatility of the framework were demonstrated by applying it to several optical configurations and investigating the impact of each change on the system's overall performance. This analysis showed that even when optimizing high-luminance LED-based lighting systems, it is imperative to consider the thermal effects in luminescent materials to accurately estimate the system's performance.

To further improve the framework's capabilities and accuracy it is necessary to obtain more precise values for the input parameters. This will require the experimental measurement of these values for different phosphors, which is proposed as future work, so that in the near future the framework can be used to obtain more realistic results with a wider variety of materials.

Acknowledgment

References

[1] V. Khanna, *Fundamentals of Solid-State Lighting*, 1st ed.   Boca Raton, FL, USA: CRC, Jun. 2014.

[2] E. F. Schubert, J. K. Kim, H. Luo, and J.-Q. Xi, "Solid-state lighting—A benevolent technology," *Rep. Progr. Phys.*, vol. 69, no. 12, pp. 3069–3099, Nov. 2006.

[3] J. J. Wierer, J. Y. Tsao, and D. S. Sizov, "Comparison between blue lasers and light-emitting diodes for future solid-state lighting," *Laser Photon. Rev.*, vol. 7, no. 6, pp. 963–993, Nov. 2013.

[4] K. A. Denault, M. Cantore, S. Nakamura, S. P. DenBaars, and R. Seshadri, "Efficient and stable laser-driven white lighting," *AIP Adv.*, vol. 3, no. 7, Jul. 2013, Art. no. 072107.

[5] T. Farooq and K. Qian, "High luminance low etendue white light source using blue laser over static phosphor," in *Proc. SPIE AOPC*, May 2015, pp. 1–6.

[6] T. Langer *et al.*, "Origin of the "green gap": Increasing nonradiative recombination in indium-rich GaInN/GaN quantum well structures," *Phys. Status Solidi*, vol. 8, no. 7/8, pp. 2170–2172, May 2011.

[7] B. Parkyn, J. Chaves, and W. Falicoff, "Remote phosphor with recycling blue-pass mirror," in *Proc. SPIE Nonimaging Opt. Efficient Illumination Syst. II*, Jul. 2005, pp. 1–12.

[8] H. Xiao *et al.*, "Improvements on remote diffuser-phosphor-packaged light-emitting diode systems," *IEEE Photon. J.*, vol. 6, no. 2, pp. 1–8, Apr. 2014.

[9] Y. Tian, "Development of phosphors with high thermal stability and efficiency for phosphor-converted LEDs," *J. Solid State Lighting*, vol. 1, no. 1, pp. 1–11, Aug. 2014.

[10] M. R. Krames *et al.*, "Status and future of high-power light-emitting diodes for solid-state lighting," *J. Display Technol.*, vol. 3, no. 2, pp. 160–175, Jun. 2007.

[11] A. Lenef, J. Kelso, Y. Zheng, and M. Tchoul, "Radiance limits of ceramic phosphors under high excitation fluxes," in *Proc. SPIE Current Develop. Lens Des. Opt. Eng. XIV*, Sep. 2013, pp. 1–20.

[12] J. K. Kim, H. Luo, E. F. Schubert, J. Cho, C. Sone, and Y. Park, "Strongly enhanced phosphor efficiency in GaInN white light-emitting diodes using remote phosphor configuration and diffuse reflector cup," *Jpn. J. Appl. Phys.*, vol. 44, no. 5L, May 2005, Art. no. L649.

[13] Y. Gu and N. Narendran, "Design and evaluation of an LED-based light fixture," in *Proc. SPIE 3rd Conf. Solid State Lighting*, Aug. 2004, pp. 318–329.

[14] P. Fulmek *et al.*, "Color temperature constancy of phosphor converted LED modules: A combined thermal and optical simulation study on the materials requirements," *E & I, Elektrotechnik und Informationstechnik*, vol. 129, pp. 1–5, Nov. 2012.

[15] F.-P. Wenzl *et al.*, "White light quality of phosphor converted LEDs from a phosphor materials perspective of view: An evaluation based on combined thermal and optical simulations," in *Proc. SPIE 12th Int. Conf. Solid State Lighting 4th Int. Conf. White LEDs Solid State Lighting*, Oct. 2012, pp. 1–7.

[16] T.-Y. Chung, S.-C. Chiou, Y.-Y. Chang, C.-C. Sun, T.-H. Yang, and S.-Y. Chen, "Study of temperature distribution within pc-WLEDs using the remote-dome phosphor package," *IEEE Photon. J.*, vol. 7, no. 2, pp. 1–11, Apr. 2015.

[17] L. Wang, S. L. Jacques, and L. Zheng, "MCML—Monte Carlo modeling of light transport in multi-layered tissues," *Comput. Method Programs Biomed.*, vol. 47, no. 2, pp. 131–146, Jul. 1995.

[18] R. Watté, B. Aernouts, and W. Saeys, "A multilayer Monte Carlo method with free phase function choice," in *Proc. SPIE Opt. Model. Des. II,* Apr. 2012, pp. 1–12.

[19] V. Bachmann, C. Ronda, and A. Meijerink, "Temperature quenching of yellow Ce 3+ luminescence in YAG:Ce," *Chem. Mater.*, vol. 21, no. 10, pp. 2077–2084, May 2009.

[20] S. Leyre, G. Durinck, J. Hofkens, G. Deconinck, and P. Hanselaer, "Experimental determination of the absorption and scattering properties of YAG:Ce phosphor," presented at the Solid-State Organic Lighting Conf., Canberra, ACT, Australia, Dec. 2014.

[21] J. Warren, S. Schaefer, A. N. Hirani, and M. Desbrun, "Barycentric coordinates for convex sets," *Adv. Comput. Math.*, vol. 27, no. 3, pp. 319–338, Aug. 2007.

[22] L.-J. Lyu and D. Hamilton, "Radiative and nonradiative relaxation measurements in Ce3+ doped crystals," *J. Lumin.*, vol. 48/49, pp. 251–254, Jul. 1991.